The Central Black Hole and Relationships with the Host Galaxy

Bradley M. Peterson

Department of Astronomy, The Ohio State University, 140 West 18th Ave., Columbus, OH 43235, USA

Abstract

More than 40 years ago, astronomers speculated that active galactic nuclei are fundamentally powered by accretion onto supermassive black holes. In this contribution, the basic observations and theoretical considerations that led to this conclusion are reviewed, as is emission-line reverberation mapping, which is now used to measure the masses of black holes in AGNs. Key correlations — the broad-line region radius–luminosity relationship and the relationships between black hole mass and host galaxy properties — are also discussed.

Key words:
accretion, black holes, reverberation mapping, host galaxies

1 Basic Properties of AGNs

1.1 Historical Perspective

The term "active galactic nucleus (AGN)" was first used by Ambartsumian (1971) to describe "violent motions of gaseous clouds, considerable excess radiation in the ultraviolet, relatively rapid changes in brightness, expulsions of jets and condensations." This was originally intended as a physical description of radio galaxies, although gradually use of the term was broadened to encompass the related phenomena of Seyfert galaxies and quasars.

Over a decade ago, I wrote an introductory textbook on AGN which, conservatively I think, stated that the term AGN referred to "the existence of energetic phenomena in the nuclei, or central regions, of galaxies which cannot be attributed clearly and directly to stars" (Peterson 1997). I chose a cautious definition because, as Blandford (1992) noted somewhat earlier, "it

remains true that, even by the lax standards of astronomy, there is no real *proof* that black holes exist in AGN, or indeed anywhere else."

Obviously a lot has changed in the last decade: there is now good evidence for the existence of supermassive black holes in galactic nuclei, at least in galaxies that have a strong spheroidal component, regardless of whether the galaxy is active or quiescent. I would suggest that a more modern definition might be that "active nuclei are those that emit radiation that is fundamentally powered by accretion onto supermassive ($> 10^6 M_\odot$) black holes." This still includes the three major types of AGNs — Seyfert galaxies, radio galaxies, and quasars — but offers an underlying physical description.

From an observational point of view, AGNs are characterized by (a) strong X-ray emission, (b) relatively strong radio emission, (c) non-stellar ultraviolet through infrared emission, and (d) broad emission lines throughout the ultraviolet, optical, and infrared. With the exception of X-ray emission, the *sine qua non* of accretion onto collapsed objects, not every AGN shares each of these characteristics: indeed, there is a phenomenological richness to AGNs, and a major focus of AGN studies in the 1980s and 1990s was AGN "unification" (discussed in more detail in this volume by Tadhunter and Elitzur), i.e., attempts to describe the diversity of AGN properties with as few parameters as possible, inclination of the system being the most important.

As already noted, there are historically three major types of AGNs: Seyfert galaxies, radio galaxies, and quasars, in order of their discovery.

- Seyfert galaxies are apparently otherwise normal galaxies that have abnormally bright central cores[1]. Seyfert (1943) identified a handful of these among nearby bright galaxies. Spectroscopy of their cores shows an unusually blue spectrum with strong, broad emission lines. Woltjer (1959) was the first to consider the physical nature of Seyfert galaxies, but they were generally treated as curiosities prior to the recognition of other types of AGNs.
- Radio galaxies were discovered when radio astronomy had progressed to where the accuracy of radio source positions allowed unambiguous identification with optical counterparts. Typically, radio galaxies show a double-lobed structure, with sizes often significantly larger than the galaxy as seen at optical wavelengths. Some sources, however, are compact, i.e., point-like at arcsecond resolution, and at the center of the optical galaxy.
- Quasars were also discovered in radio surveys, though their nature was not immediately clear. Some radio sources, particularly those at high Galactic

[1] Seyfert galaxies are really quite striking when observed directly through a telescope. Even through large telescopes, galaxies have an amorphous appearance. Seyfert galaxies, however, look as though there is a bright star superposed on the very center of the galaxy.

latitude and therefore probably extragalactic, were identified with star-like optical sources, although there often appeared to be "fuzz" around these objects or sometimes jet-like features associated with them (i.e., they were not *really* completely star-like in appearance). The optical spectra of these sources were confusing, but they were clearly not normal stars. They were thus referred to as "quasi-stellar radio sources," a name that was ultimately contracted to "quasar."

The first breakthrough in unlocking the enigmatic nature of quasars came when Schmidt (1963) recognized that the emission lines in the spectrum of the quasar 3C 273 were in fact the Balmer lines [2] at the then-astounding redshift of $z = 0.158$. The redshift itself was not so spectacular, as the more distant Abell clusters of galaxies were known to have redshifts as high as $z \approx 0.2$; however, the most luminous cluster galaxies have apparent magnitudes $B \approx 18\,\mathrm{mag}$, while the apparent magnitude of 3C 273 is $B = 13.1\,\mathrm{mag}$! If 3C 273 is at the cosmological distance indicated by its redshift, it must be ~ 100 times as luminous as the brightest galaxies.

Yet another surprise followed: these very luminous sources were found to be highly variable at every wavelength at which they could be observed. Significant flux variations were observed on timescales as short as days. Because the flux variations are of large amplitude, whatever the physical cause of the variations, a correspondingly large fraction of the source must be involved, i.e., the source is varying "coherently." And since the varying parts of the source must be causally connected, the maximum speed at which the variability signal can propagate through the region, the speed of light, sets an upper limit on the size of the source, which in the case of quasars is of order light days. Explaining how a region the size of the Solar System can produce the light of a trillion stars was the challenge facing astronomers at the time. This was the genesis of a two-decade controversy on the nature of quasars: are they really at cosmological distances and ridiculously compact and luminous, or are their redshifts due to some effect other than cosmological expansion and quasars themselves are relatively nearby and less luminous than required in the cosmological interpretation?

In retrospect, one might ask why the connection between Seyfert galaxies and

[2] To the contemporary reader, it probably seems surprising that it took so long to identify the Balmer lines, even if shifted by $\sim 16\%$. One must remember, though, these spectra were photographic: the response of photographic material to light is roughly logarithmic with intensity, so the contrast between the lines and continuum is less than in spectra produced with modern linear detectors. Also, such broad emission lines are rarely encountered elsewhere in astrophysics — indeed, upon inspection of a photographic spectrum of a quasar, it's hard to tell whether you are looking at broad emission lines or an absorption spectrum with very broad features, such as those in a white dwarf.

quasars was not made at this time? It certainly would have settled the redshift controversy more rapidly. Our modern view is that the distinction between these two types of object is rather arbitrary: quasars are merely higher luminosity versions of Seyfert galaxies. Weedman (1976) argues that the failure to recognize this early on was because at the time the first quasars were discovered, the original Seyfert galaxies and the relatively few known quasars all represented extremes of their particular class: Seyfert galaxies are nearby spiral galaxies with abnormally bright cores, and quasars are distant unresolved, high-luminosity, variable radio sources. It was only after identification of large numbers of Seyfert-like and quasar-like objects that it became apparent that they were physically related.

1.2 Searching for Quasars

Because of their extraordinary properties, quasars immediately drew the attention of many astronomers. In the early 1960s, only a bare handful of quasars were known. These were radio sources whose positions had been accurately established by lunar occultations or by interferometry. Most radio source positions were accurate only to arcminute levels (the diffraction limit for single-dish antennas), although one could identify the quasar in a high-Galactic latitude field by laboriously obtaining spectra of the likely candidates in the field. However, it quickly became apparent that there was a more economical way to identify quasars: quasars are very blue compared to stars, especially in the near ultraviolet, shortward of the Balmer limit. When plotted on a two-color diagram, $U-B$ vs. $B-V$, quasars stand out as a distinct population from stars, making it easy to identify them[3]. It quickly became apparent that identifying "quasar candidates" (since only spectroscopy could confirm their identification as quasars and yield their redshifts) by their "ultraviolet (UV) excess" alone might be the most efficient way to find them. Indeed, spectroscopy of UV-excess sources at high Galactic latitude revealed that the surface density of quasar-like sources was higher than the surface density of radio sources (Sandage 1965). While most UV-excess sources turn out to be Galactic white dwarfs or horizontal branch stars, it is true that the "radio-quiet" versions of quasars are 10 to 20 times as numerous as the "radio-loud" variety. The radio-quiet variety were referred to as "quasi-stellar objects" (QSOs) to distinguish them from the radio-loud quasars. This distinction is rarely made today.

[3] Note that the particular photometric system in common use, the Johnson *UVB* system, is effective at isolating low-redshift quasars. Other multiband systems, such as that designed for the Sloan Digital Sky Survey, are more useful for finding quasars over a wide range of redshifts.

As the number of known AGNs grew, various subclasses emerged. One of the most important is the distinction between two spectroscopically defined varieties of Seyfert galaxy, first recognized by Khachikian & Weedman (1974). Spectra of "type 1" Seyfert galaxies show that the permitted emission lines (like the Balmer series) have broad components that have widths corresponding to Doppler broadening typically around $5000\,\mathrm{km\,s^{-1}}$. Forbidden lines, like [O III] $\lambda\lambda$4959, 5007, however, are much narrower, with widths typically $\sim 500\,\mathrm{km\,s^{-1}}$. Permitted lines also have a narrow component that is superposed on the broad feature. The spectra of "Seyfert 2" galaxies have only the forbidden lines and the narrow components of the permitted lines visible.

Another manifestation of the AGN phenomenon that always seems to cause confusion on first encounter is the subclass of Type 1 objects known as "narrow-line Seyfert 1" (NLS1) galaxies (Osterbrock & Pogge 1986). The optical spectra of these objects show permitted lines that are only marginally larger than the narrow-line components; one criterion for inclusion in this subclass is permitted line widths FWHM $< 2000\,\mathrm{km\,s^{-1}}$. Another criterion is the flux ratio [O III] $\lambda5007/\mathrm{H}\beta > 3$, to distinguish these sources from Type 2 Seyferts. That NLS1s are true type 1 objects is demonstrated by the presence of strong Fe II emission blends on either side of Hβ — these features are seen only in Seyfert 1 spectra.

Another related group of objects are "low-ionization nuclear emission region" (LINER) galaxies. Spectroscopically, LINERs are similar to Seyfert 2 galaxies, except that their lower-ionization level emission lines are relatively more prominent. In both LINERs and Seyfert 2s, however, the presence of high-ionization lines indicates photoionization by a hard spectrum, not simply hot stars.

The final subclass of AGN that we will introduce here are "BL Lac objects" [4]. Like other quasars, BL Lac objects are strong radio sources and are very blue in the optical. They are also among the most highly variable AGNs. What distinguishes them from other AGNs is the weakness of the emission and absorption lines in their spectra — their optical spectra appear to be nearly featureless. Their extreme flux variability is shared by some extreme quasars, "optically violent variables," which have otherwise typical quasar emission-line spectra. Together, BL Lacs and optically violent variables are sometimes referred to as "blazars."

[4] The name "BL Lacertae" is a variable star designation. The archetype of this class was originally erroneously identified as a variable star prior to its detection as a radio source.

For the last 25 years, a major theme of AGN studies has been "unification," which is based fundamentally on Occam's razor — the best description of AGNs is likely to be the simplest one that explains all the data. In other words, we desire to explain the broad range of observed AGN properties and types with as few parameters as possible.

The picture that has emerged is of a central black hole that is surrounded by an accretion disk. Thermal emission from the disk accounts for most of the UV/optical continuum. The outer part of the accretion disk is probably the inner edge of the broad-line region (BLR) that produces the strong, broad emission lines. The BLR geometry is unknown, but a great deal of circumstantial evidence suggests that it has a disk-like component and probably also a disk-wind arising from it. The outer edge of the BLR seems to be defined by the dust-sublimation radius, i.e., the nearest point to the central source where dust can survive. The dust-sublimation radius also defines the inner edge of a mostly opaque dusty structure that is usually described as a "torus" (though see the contribution of Elitzur in this volume for a more sophisticated discussion). All of this is embedded in a much larger region, up to 100s of parsecs, of low-density gas, the "narrow-line region" (NLR), which produces the narrow forbidden lines and permitted line cores. In addition to this, radio jets are sometimes observed on various scales along the axis of the system.

The key ingredient in AGN unification is the dusty torus that surrounds the central source and the BLR. If we observe this system from a vantage point along the system axis, we see radiation from the central source and the BLR, as well as the NLR, i.e., we will observe a type 1 spectrum. On the other hand, in the system plane, we see only the NLR directly, and if we see the central source and BLR at all, it is via scattering. In this case, we will observe a type 2 spectrum.

Details of unification models are discussed more thoroughly elsewhere in this volume.

2 The Central Engine

Very early on, it was obvious that only gravitational accretion onto supermassive ($> 10^6\,M_\odot$) collapsed objects could produce the amount of luminous energy required in the cosmological interpretation of quasar redshifts (Zel'dovich & Novikov 1964; Salpeter 1964; Lynden-Bell 1969). The argument is very straightforward, only that the self-gravity of the source must exceed

the outward radiation pressure for the source to maintain its physical integrity. The outward energy flux in radiation at a distance r from the central source of luminosity L is

$$F = \frac{L}{4\pi r^2}. \tag{1}$$

Since the momentum of a photon of energy E is $p = E/c$, the momentum flux, or pressure, in photons is

$$P_{\rm rad} = \frac{F}{c} = \frac{L}{4\pi c r^2}. \tag{2}$$

The force experienced by a particle of cross-section σ is thus

$$F_{\rm rad} = P_{\rm rad}\sigma = \frac{L\sigma}{4\pi c r^2}. \tag{3}$$

In the intense UV radiation field of an AGN, it is reasonable to assume that matter is completely ionized so the relevant cross-section is the Thomson cross-section for electron scattering, $\sigma_e = 6.65 \times 10^{-25}\,{\rm cm}^2$. Now requiring that this force is less than the gravitational force on the ionized gas, we have the condition

$$\frac{L\sigma_e}{4\pi c r^2} \leq \frac{GMm_p}{r^2}, \tag{4}$$

which can be rearranged to

$$L \leq \frac{4\pi G c m_p}{\sigma_e} M \approx 1.26 \times 10^{38} \left(\frac{M}{M_\odot}\right)\ {\rm ergs\ s^{-1}}. \tag{5}$$

The highest luminosity a source of mass M can have and still be stable against radiation pressure is known as the "Eddington limit," $L_{\rm Edd} = 1.26 \times 10^{38}\,(M/M_\odot)$ ergs s^{-1}. Equation (5) shows that a luminous Seyfert nucleus with $L \approx 10^{44}\,{\rm ergs\ s^{-1}}$ must have a mass in excess of $\sim 10^6\,M_\odot$.

It is also simple to estimate the rate at which mass must be accreted to account for the radiant output of AGNs. We will assume that the energy that can be extracted from a particle of mass M is some fraction of its rest energy $E = \eta M c^2$, where η is an efficiency factor. The rate at which energy is extracted is globally

$$L = dE/dt = \eta \dot{M} c^2 \tag{6}$$

where $\dot{M} = dM/dt$, which we can identify as the mass accretion rate.

To estimate the efficiency of conversion of gravitational potential energy, we note that the potential energy of a mass M at a distance r from a black hole of mass $M_{\rm BH}$ is $U = GM_{\rm BH}M/r$. We will show below that the UV/optical continuum arises primarily at a distance $r \approx 10R_g$, where $R_g = GM_{\rm BH}/c^2$ is the gravitational radius of the black hole. The potential energy available is thus

$$U = \frac{GM_{\rm BH}M}{10R_g} = 0.1Mc^2. \tag{7}$$

The rate at which we convert this to radiant energy can be taken to be $dU/dt = 0.1\dot{M}c^2$, and comparison with equation (6) suggests that $\eta \approx 0.1$ for accretion onto a black hole. The appeal of gravitational attraction as the driving force in AGNs is this high efficiency (compared to, say, the proton-proton fusion chain, for which $\eta = 0.007$, or common chemical reactions, for which $\eta \approx 10^{-9}$). Using equation. (6) with $\eta = 0.1$, we see that the accretion rate needed to sustain a $L = 10^{46}\,{\rm ergs\ s^{-1}}$ quasar is only $\sim 2M_\odot\ {\rm yr^{-1}}$. This "Eddington rate" is the mass accretion rate necessary to sustain the Eddington luminosity, i.e.,

$$\dot{M}_{\rm Edd} = \frac{L_{\rm Edd}}{\eta c^2} \approx 1.4 \times 10^{18}(M/M_\odot)\ {\rm gm\ s^{-1}}. \tag{8}$$

It is also sometimes useful to use the "Eddington ratio" to express the actual accretion rate relative to the Eddington rate, i.e., $\dot{m} = \dot{M}/\dot{M}_{\rm Edd}$.

2.1 Evidence for Supermassive Black Holes

The arguments above certainly make it clear why invoking supermassive black holes to power quasars was extremely attractive, but compelling evidence for massive collapsed objects at the centers of galaxies has been lacking until relatively recently.

The nearest and best-studied supermassive black hole is that at the center of our own Milky Way Galaxy, a quiescent (i.e., $\dot{m} \approx 10^{-7}$) galaxy. Infrared imaging has allowed measurement of proper motions of multiple stars in the vicinity of the $3.7\ (\pm 0.2) \times 10^6\,M_\odot$ black hole at the Galactic Center (Schödel et al. 2003; Ghez et al. 2005).

The other very well-established black hole mass is in an active galaxy, the Seyfert 2 galaxy NGC 4258. In this AGN, the black hole is surrounded by a warped gas disk containing H_2O megamasers. Dynamical modeling of their

radial velocities and proper motions, determined in exquisite detail with VLBI monitoring, reveal a central mass of $3.9 \times 10^7\, M_\odot$ (Miyoshi et al. 1995; Herrnstein et al. 1999).

Masses of black holes have been measured for about three dozen relatively nearby galaxies based on dynamical modeling of stars or gas disks in the nucleus. The challenge in this work is that it requires sufficiently high angular resolution to resolve the black hole "radius of influence" $R_{\rm BH} = GM_{\rm BH}/\sigma_*^2$, where σ_* is the velocity dispersion of the stars in the bulge of the galaxy.

The forty or so quiescent galaxies whose central black hole masses have been measured show two remarkable correlations between the black hole mass and global properties of the galaxies: (1) a correlation between black hole mass and bulge luminosity, the $M_{\rm BH}$–$L_{\rm bulge}$ relationship, or equivalently, between black hole mass and bulge mass, the $M_{\rm BH}$– $M_{\rm bulge}$ relationship (Kormendy & Richstone 1995), and (2) a correlation between black hole mass and bulge stellar velocity dispersion (Ferrarese & Merritt 2000; Gebhardt et al. 2000a), known as the $M_{\rm BH}$–$\sigma*$ relationship. Both of these correlations are rather extraordinary because they link the properties of the black holes, which constitute only $\sim 0.2\%$ of the bulge mass, with the larger-scale properties of the galaxies. The latter correlation seems to have very little intrinsic scatter, and the former correlation is also very tight if the bulge light is measured in the infrared (Marconi & Hunt 2003).

In the case of AGNs, masses are generally determined by reverberation mapping, which we will describe in detail below. Reverberation mapping measures the size R of the BLR by determining the time delay between continuum and emission-line variations due to light-travel time across the BLR. By combining this with the emission-line width ΔV, one can determine the enclosed mass. The evidence that this process is actually measuring the mass of the central black hole is threefold:

(1) When multiple emission-line time delays are measured in a single object, the broader lines have shorter time delays than the narrower lines. Indeed, one finds that the "virial product" $\Delta V^2 R/G$ is constant, suggesting that gravity is the dominant force on the gas.
(2) AGN host galaxies with reverberation-based black hole masses show a $M_{\rm BH}$–σ_* relationship; indeed, the $M_{\rm BH}$–σ_* relationship is used to provide a zero-point calibration for the reverberation-based black hole mass scale.
(3) In the very few cases where stellar dynamical or gas dynamical mass measurements are available for reverberation-mapped AGNs, there is consistency between the results. It is worth noting, however, that the tests are not yet very critical as stellar dynamical and gas dynamical measurements are extremely challenging in the case of AGNs and individual reverberation-based black hole masses are systematically uncertain by a

factor of a few.

We will return to this in some detail later.

2.2 Accretion Disks

As gas falls into the black hole, viscosity and any residual angular momentum will result in the formation of an accretion disk. The simplest sort of accretion disk structure is geometrically thin and optically thick, so that it radiates locally like a blackbody (Shakura & Sunyaev 1973). As matter spirals into the black hole, half of the potential energy is released into radiation so the luminosity of the disk is

$$L = \frac{GM_{\rm BH}\dot{M}}{2r} = 2\pi r^2 \sigma T^4, \tag{9}$$

where T is the temperature at radius r, σT^4 is the luminosity per unit area, and the radiating area of the disk is $2\pi r^2$, where the factor of two enters because the disk is two-sided. We can rearrange this as

$$T(r) = \left(\frac{GM_{\rm BH}\dot{M}}{4\pi\sigma r^3}\right)^{1/4}. \tag{10}$$

This encapsulates the essential physics, but a more careful and complete derivation would yield

$$T(r) = \left[\frac{3GM_{\rm BH}\dot{M}}{8\pi\sigma r^3}\left\{1 - \left(\frac{R_{\rm in}}{r}\right)^{1/2}\right\}\right]^{1/4}, \tag{11}$$

where $R_{\rm in}$ is the inner radius of the disk. For $r \gg R_{\rm in}$, some substitution yields

$$T(r) \approx 3.7 \times 10^5 \ \dot{m}^{1/4} \left(\frac{M_{\rm BH}}{10^8 M_\odot}\right)^{-1/4} \left(\frac{r}{R_g}\right)^{-3/4} \ {\rm K}. \tag{12}$$

The spectral energy distributions of quasars typically peak at a rest wavelength $\sim 1000\,$Å, and Wien's Law tells us that corresponds to the peak of emission for a blackbody of temperature $T \approx 5 \times 10^5$ K. For a $10^8\,M_\odot$ black hole with $\dot{m} \approx 0.1$ (a typical value, as we will see), equation (12) tells us that the emission will peak at $\sim 7R_g$ (we used $10R_g$ earlier).

It should be emphasized that this is a gross oversimplification. Such a simple model significantly under-predicts the X-ray emission, which apparently arises

in a hot corona above the disk. The thin-disk model also predicts that the UV-optical spectrum ought to have a spectral shape $L_\nu \propto \nu^{1/3}$, which is not what is observed. Finally, accretion disks are subject to several instabilities; these probably account for the observed continuum variability of AGNs.

2.3 Continuum Variability

Variability at all wavelengths is a signature property of AGNs. From the infrared to X-rays, AGNs tend to show larger variations at shorter wavelengths. The variations are aperiodic and therefore unpredictable. They can be characterized in terms of a power-density spectrum $P(f) \propto f^{-\alpha}$ where f is the temporal frequency. The index is typically in the range $1 \leq \alpha \leq 2.5$, i.e., the amplitude of variation is larger over larger time intervals. The ultimate cause of the flux variations is not known, but is probably attributable to disk instabilities that alter the accretion rate. Kawaguchi et al. (2000) have argued that the power-density spectra of AGNs are consistent with magnetohydrodynamical instabilities (disconnection events). In some special cases, variability might be attributable to variable obscuration of the central source or by gravitational microlensing by stars.

3 Reverberation Mapping: Black Hole Masses and Connections with Host-Galaxy Properties

3.1 Emission-Line Variability

The first report of broad emission-line variability was by Andrillat & Souffrin (1968) who showed a dramatic change in the strength of the Hβ emission line in the Seyfert 1 galaxy NGC 3516 from Seyfert's (1943) original observation. There were assorted reports of similar variations, but most of these were widely disregarded because of the difficulty of doing accurate spectrophotometry with photographic detectors. Even with some reliable reports in the 1970s based on spectra obtained with high-quality electronic detectors (e.g., Tohline & Osterbrock 1976; Phillips 1978), emission-line variability was seen by most astronomers as a curiosity. It was only with the proliferation of electronic detectors on 2-m class telescopes and with the advent of the *International Ultraviolet Explorer (IUE)*, which was launched in 1978, that studies of AGN emission-line variability were undertaken in earnest.

It is worth recalling what was known about the BLR around 1980. At that time, the only available size estimate for the BLR was theoretical, based on

photoionization equilibrium calculations. Photoionization models are characterized by (1) the shape of the ionizing continuum, (2) the elemental abundances of the gas, (3) the particle density of the gas n_H, and an ionization parameter

$$U = \frac{Q_{\rm ion}({\rm H})}{4\pi r^2 n_H c}, \tag{13}$$

where the rate at which the central source, at a distance r from the gas, produces hydrogen-ionizing photons is

$$Q_{\rm ion}({\rm H}) = \int \frac{L_\nu}{h\nu}\, d\nu, \tag{14}$$

where L_ν is the specific luminosity of the ionizing source and the integral is over all ionizing frequencies. The ionization parameter U thus reflects the ratio at which photoionizations occur, which is obviously proportional to $Q_{\rm ion}({\rm H})$, and the rate at which recombinations occur, which is proportional to n_H. In the case of the BLR, the particle density was assumed to be constrained by the absence of all forbidden lines except for C III] λ1909, which is collisionally suppressed at densities in excess of $\sim 3 \times 10^9\,{\rm cm}^{-3}$. At this density, photoionization modeling of AGNs matches the C III] to C IV λ1549 flux ratio for a value of $U \approx 0.01$ (e.g., Ferland & Mushotzky 1982). Using these values for a Seyfert 1 galaxy such as NGC 5548 (with $L_{\rm bolometric} \approx 10^{44}\,{\rm ergs\ s}^{-1}$), equation (13) yields an estimate of the size of the BLR $r \approx 130$ light days. Equation (13) further suggests that the size of the BLR should scale with luminosity as $r \propto L^{1/2}$, since to some low order of approximation, the emission-line spectra of AGNs are very similar over a wide range of luminosity, suggesting that U and n_H are similar [5].

Given the predicted large size of the BLR, emission-line variability was not necessarily expected, certainly not on short time scales. Short time scale emission-line profile variations were observed and attempts were made to explain these as excitation inhomogeneities due to short timescale variations. This led a number of researchers to resurrect an earlier idea of Bahcall, Salpeter, & Koslovsky (1972) that the geometry of the BLR could be traced by examining how these excitation inhomogeneities propagated through the BLR (Fabrika 1980; Blandford & McKee 1982; Capriotti, Foltz, & Peterson 1982; Antohkin & Bochkarev 1983). Blandford & McKee provided the essential formalism and the name for this process, "reverberation mapping."

[5] This is not strictly true, but only one strong luminosity effect seems to exist, namely that the strength of the C IV λ1549 relative to the underlying continuum (i.e., the equivalent width of the line) decreases with increasing luminosity. This is known as the Baldwin Effect (Baldwin 1977).

The first concerted efforts to determine the size of the BLR were frustrated by overestimates of the size of the BLR that led to under-sampling the light curves. A European effort led by Michael Penston and Marie-Helene Ulrich observed NGC 4151 with *IUE* every 2 – 3 months (Ulrich et al. 1991 and references therein). Antonucci & Cohen (1983) also observed NGC 4151 approximately monthly during 1980 and 1981 at Lick Observatory. Peterson et al. (1983, 1985) monitored Akn 120 once per month for several observing seasons and were the first to suggest that the BLR might be much smaller than previously supposed. Whether or not this specific conclusion was correct was disputed, but it was certainly clear by the late 1980s that higher sampling rates over long duration were going to be required to measure emission-line time delays. It was quickly realized that such massive efforts would require large-scale international cooperation, which led to the establishment of the International AGN Watch, a large informal consortium that was formed to coordinate monitoring programs. The AGN Watch carried out its first successful program in 1988–89 with *IUE* and ground-based telescopes (Clavel et al. 1991; Peterson et al. 1991). At about the same time, other groups were starting to carry out similar intensive programs from the ground.

3.2 Reverberation Mapping: Theory

Early observations of emission-line variability, as described above, allow us to draw some important preliminary conclusions (see Peterson 1993 for additional details). First, the light-travel time across the BLR must be rather short, at least for nearby Seyfert galaxies, since significant variability is detected on time scales as short as weeks. Furthermore the gas must be relatively dense so that the recombination time is short; however, we have already concluded that the particle density of the BLR must be $n_e \approx 3 \times 10^9\,\mathrm{cm}^{-3}$ and since the recombination timescale is $\tau_{\rm rec} \approx (n_e \alpha_{\rm B})^{-1}$, where $\alpha_{\rm B}$ is the hydrogen recombination coefficient, in the BLR, $\tau_{\rm rec} \approx 20\,\mathrm{min}$. An important result that was quite a surprise to theorists is that the clear correlation between the emission-line variations and optical or satellite UV continuum variations implies that the continuum variations at observable wavelengths must be closely coupled to variations in the hydrogen-ionizing continuum at wavelengths $\lambda < 912\,\text{Å}$ (Courvoisier & Clavel 1991; Collin-Souffrin 1991). The conclusion that, whatever the origin of continuum variability, the signal must propagate through the continuum-emitting region at close to the speed of light seems inescapable.

In describing how the broad emission lines respond to continuum variations, we generally make some simplifying assumptions that can be justified *ex post facto*:

(1) It is assumed that the continuum originates in a single central source that

is small compared to the BLR. This point-source assumption[6] is quite reasonable since the UV/optical continuum arises at $\sim 10\,R_g$, and the broad lines are found to arise at distances larger than $\sim 1000\,R_g$.

(2) The light travel time scale $\tau_{\rm LT} = R_{\rm BLR}/c$ is the most important timescale, much shorter than the dynamical time scale $\tau_{\rm dyn} = R_{\rm BLR}/\Delta V$ and much longer than the recombination time.

(3) There is a simple, though not necessarily linear or instantaneous, relationship between the ionizing continuum that drives the emission-line variations and the observable UV/optical continuum, and that for small variations, we can approximate the emission-line response as linear.

Under these assumptions, the response of an emission line to a variable continuum $C(t)$ at line-of-sight (or Doppler) velocity $V_{\rm LOS}$ at time t is

$$L(V_{\rm LOS}, t) = \int \Psi(V_{\rm LOS}, \tau)\, C(t-\tau)\, d\tau, \tag{15}$$

where by inspection we can see that the "transfer function" or "velocity-delay map" $\Psi(V_{\rm LOS}, \tau)$ is the observed response to a delta-function continuum outburst. Obviously, the velocity-delay map depends on the structure and dynamics of the BLR, and in all but trivial cases, on the inclination of the BLR relative to the observer.

It is instructive to construct from first principles a velocity-delay map for a simple system. The approach we should take, obvious from consideration of equation (15), is to project into the observable coordinates $(V_{\rm LOS}, \tau)$ the response of the system to a delta-function outburst. At any given time delay τ following the outburst, the locus of points that the observer will see responding to the outburst lie along an "isodelay surface" for which the light travel time from the continuum source to the responding gas to the observer is constant: it is trivially concluded that the isodelay surface must be an ellipse, or given that the observer is at such a large distance from the system, a parabola. The observer will see different parts of the line-emitting region respond as the continuum pulse propagates through the BLR along isodelay surfaces.

For simplicity, consider a BLR (or an element of a BLR) that is a ring of line-emitting clouds in a circular Keplerian orbit around the central black hole at an inclination of 90° (i.e., edge-on) to the observer, as shown in Figure 1. In the top panel of Figure 1, we show an arbitrary isodelay surface that intersects the ring of BLR clouds at two locations, each at an angle θ from the line of sight as seen from the central source. At these two locations, the observed line-of-sight velocity is $\pm v_{\rm orb} \sin\theta$, where the orbital speed is $v_{\rm orb} = (GM_{\rm BH}/R)^{1/2}$.

[6] It is worth mentioning that the point-source assumption cannot be made in reverberation-mapping of the Fe Kα line at 6.4 keV, which greatly complicates the process (Reynolds et al. 1999).

The time delay for this isodelay surface is given by the length of the dotted line in the top panel of Figure 1, $(1 + \cos\theta)R/c$. The bottom panel of Figure 1 shows how this ring of line-emitting clouds projects into the observable velocity-time delay space: a ring in configuration space projects to an ellipse in velocity-time delay space, extending from a time delay $\tau = 0$ (at $\theta = 180^{\rm o}$) to $\tau = 2R/c$ (at $\theta = 0^{\rm o}$) and line of sight velocities $\pm v_{\rm orb}$ (at $\theta = \pm 90^{\rm o}$). On the basis of symmetry arguments or by direct computation, the average time delay for a ring is $\langle\tau\rangle = R/c$. The width of the velocity-delay map for a ring can be characterized by a number of different parameters, among the more useful being the full width at half maximum (FWHM) and the line dispersion, defined as

$$\sigma_{\rm line} = \left(\langle V_{\rm LOS}^2\rangle - \langle V_{\rm LOS}\rangle^2\right)^{1/2}. \tag{16}$$

By symmetry, $\langle V_{\rm LOS}\rangle = 0$, and it can be shown that $\sigma_{\rm line} = v_{\rm orb}/2^{1/2}$.

Extending this to more plausible geometries is straightforward. A Keplerian disk, for example, is simply a series of infinitesimal rings, each projecting to an ellipse with the time-delay axis proportional to R and the line-of-sight velocity axis proportional to $R^{-1/2}$. A velocity-delay map for a disk is illustrated in Figure 2. The multiple-ring type structure is apparent, as is the Keplerian taper towards longer time delays (or larger orbits). Also shown in the Figure is the projection of the velocity-delay map into time delay alone by integrating over all velocities and in the emission-line profile, obtained by integrating over all time delays.

3.3 Reverberation Mapping: Practice

Observationally, the goal of reverberation mapping is to obtain a long series of measurements of continuum $C(t)$ and velocity-resolved emission-line fluxes $L(V_{\rm LOS}, t)$, solve for the velocity-delay map using equation (15), and thus discern the geometry, velocity field, and inclination of the BLR as reflected in a particular emission line. By observing multiple lines that arise in gases of different levels of ionization, it should be possible to map out the entire BLR.

Unfortunately, doing this in practice turns out to be extremely difficult. AGNs are faint so the data tend to be noisy. Telescope time is a limited commodity so the time resolution and duration of the experiment are often suboptimal. Variations tend to be small on the short time scales that must be sampled to attain high spatial resolution, and spectrophotometry accurate at the 1% level or so is just plain hard to achieve. As a result, attempts to recover velocity-delay maps from existing data have had very limited success. Published velocity delay maps (e.g., Ulrich & Horne 1996; Kollatschny 2003a) are quite noisy

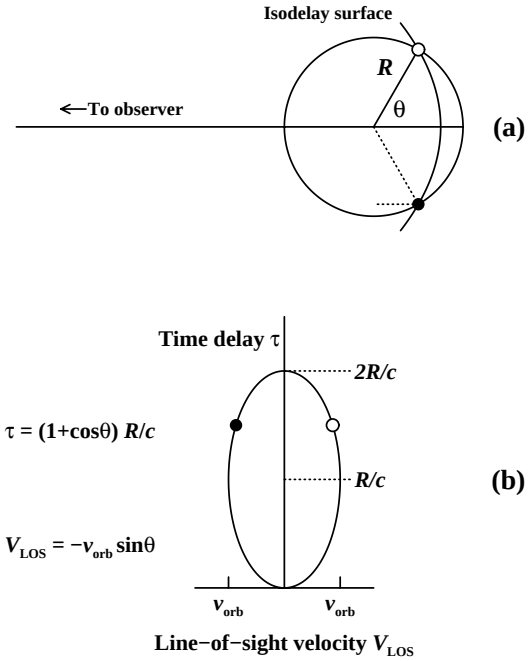

Fig. 1. The upper diagram shows a ring (or cross-section of a thin shell) that contains line-emitting clouds. An isodelay surface for an arbitrary time is given; the intersection of this surface and the ring shows the clouds that are observed to be responding at this particular time. The dotted line shows the additional light-travel time, relative to light from the continuum source, that signals reprocessed by the cloud into emission-line photons will incur, $\tau = (1+\cos\theta)R/c$. In the lower diagram, we project the ring of clouds onto the line-of-sight velocity/time-delay $(V_{\rm LOS}, \tau)$ plane, assuming that the emission-line clouds in the upper diagram are orbiting in a clockwise direction (so that the cloud represented by a filled circle is blueshifted and the cloud represented by an open circle is redshifted).

and show little clear evidence for structure. Detailed simulations (Horne et al. 2004), however, show that the data requirements to obtain a high-fidelity velocity-delay map are within current capabilities.

Even though the ultimate goal of recovering a high-fidelity velocity-delay map has not yet been achieved, it has been possible to measure the mean response times for several emission lines in a few sources and for the Balmer lines in many sources. An accurate mean time delay for any particular emission line is

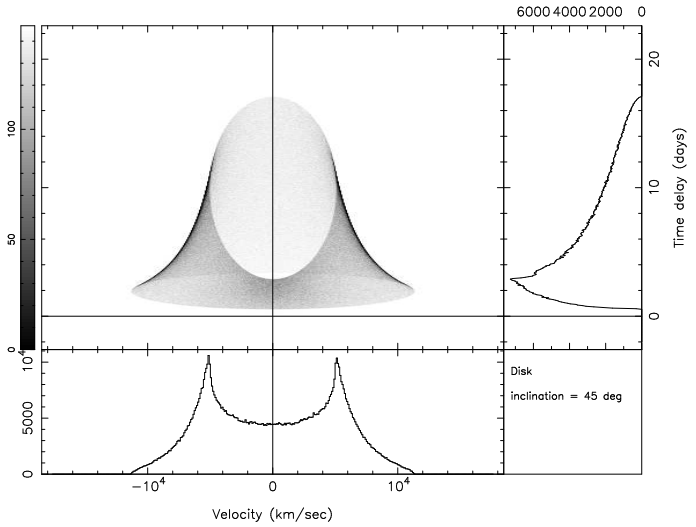

Fig. 2. Velocity–delay map for a thin disk at inclination $i = 45^{\rm o}$. The upper left panel shows in gray scale the velocity–delay map, i.e., the transfer function or the observed emission-line response as a function of line-of-sight velocity $V_{\rm LOS}$ and time delay τ. The upper right panel shows the one-dimensional transfer function, i.e., the velocity–delay map integrated over $V_{\rm LOS}$, which is the response of the total emission line as a function of time. The lower left panel shows the emission-line response integrated over time delay; this is the profile of the variable part of the line.

easily measured by cross-correlation of the continuum and emission-line light curves. Since cross-correlation of two irregularly sampled time series presents a number of technical problems, exactly how this has been done in practice merits some attention. We conventionally assume that the two time series are related linearly and thus compute the standard linear correlation coefficient r between pair-wise points (x_i, y_i) as

$$r = \frac{\sum_i \left(x_i - \langle x \rangle\right)\left(y_i - \langle y \rangle\right)}{\left(\sum_i \left[x_i - \langle x \rangle\right]^2\right)^{1/2} \left(\sum_i \left[y_i - \langle y \rangle\right]^2\right)^{1/2}} \tag{17}$$

where $\langle x \rangle$ and $\langle y \rangle$ are the means of their respective series. This definition of the correlation coefficient has a value of $r = 1$ for two perfectly correlated series, $r = -1$ for a perfect anti-correlation, and $r = 0$ for completely uncorrelated data. In applying this to two time series $C(t)$ and $L(t)$, we compute the linear correlation coefficient by pair-wise matching the series for different time delays τ, i.e., $x = C(t - \tau), y = L(t)$ to determine the value of τ that maximizes the linear correlation between the two series. The challenge in cross-correlating the two time series is that the spacing between observations is generally not regular: in the ideal case, each series is sufficiently well-sampled that for every emission-line measurement $L(t)$ there is a corresponding continuum observation $C(t - N\Delta\tau)$, where N is an integer and $\Delta\tau$ is the sampling interval between observations. If the interval between observations is not a constant, then for each measurement $L(t)$ there is not always an actual measurement

$C(t-\tau)$ for arbitrary τ. There are basically two ways to deal with this:

- For any arbitrary shift τ, a real data point in one series $L(t)$ can be pair-wise mapped to a value $C(t-\tau)$ by interpolation of the light curve $C(t)$ (Gaskell & Sparke 1986; Gaskell & Peterson 1987). This poses some dangers if the time-sampling is poor, but if the sampling is reasonably good, the results are quite reliable (White & Peterson 1994). Usually simple linear interpolation between the real data points on either side of the interpolated point is sufficient and higher-order interpolation affords no particular advantage.
- Instead of interpolating, a real data point in one series $L(t)$ can be pair-wise mapped to any real data points in the interval $\tau - \Delta\tau/2$ to $\tau + \Delta\tau/2$, i.e., a "discrete correlation function" (DCF) with time bins of width $\Delta\tau$ (Edelson & Krolik 1988; Alexander 1997). The DCF can be very valuable in cases where interpolation might be risky, such as when there are large gaps in the time series (e.g., Peterson et al. 2005). On the other hand, for well-sampled time series, the time resolution attainable with the DCF is poorer than obtainable by the interpolation method (White & Peterson 1994).

One of the more contentious issues that arose in analyzing reverberation data was how to assess uncertainties in measured lags. For the past decade, the standard has been to make use of model-independent Monte Carlo simulations that randomly sample a subset of the data and then randomly re-adjust the measured fluxes assuming that their uncertainties are Gaussian distributed (Peterson et al. 1998). The errors in the lags are assessed by carrying out a large number of realizations, measuring the lag for each case, and then using the distribution of lags from the simulations to identify the mean and standard deviation.

Additional details on methodology are provided by Peterson (2001).

3.4 Reverberation Mapping: Results

Arguably the most successful reverberation mapping program was the first combined *IUE*/ground-based program by the International AGN Watch almost 20 years ago (Clavel et al. 1991; Peterson et al. 1991). This was an eight-month campaign anchored by UV spectra obtained once every four days by *IUE*. Ground-based spectroscopy was obtained by nearly 20 different telescopes with an even higher sampling rate. Table 1 shows the lags measured from the data obtained in this campaign (as remeasured by Peterson et al. 2004). Lags for the features listed in column (1) are relative to the UV continuum variations at ~ 1350 Å. Column (2) gives the amplitude of variability

Table 1
Reverberation Results for NGC 5548

Feature	$F_{\rm var}$	Lag (days)
UV continuum	0.321	—
Optical continuum	0.117	$0.6^{+1.5}_{-1.5}$
He II λ1640	0.344	$3.8^{+1.7}_{-1.8}$
N V λ1240	0.411	$4.6^{+3.2}_{-2.7}$
He II λ4686	0.052	$7.8^{+3.2}_{-3.0}$
C IV λ1549	0.136	$9.8^{+1.9}_{-1.5}$
Lyα λ1215	0.169	$10.5^{+2.1}_{-1.9}$
Si IV λ1400	0.185	$12.3^{+3.4}_{-3.0}$
Hβ λ4861	0.091	$19.7^{+1.5}_{-1.5}$
C III] λ1909	0.130	$27.9^{+5.5}_{-5.3}$

as an rms fractional variation, corrected for measurement uncertainties[7], and column (3) gives the lag for each feature in units of days.

It is obvious from these results is that the BLR is significantly smaller than expected on the basis of photoionization equilibrium models. Equally obvious is the evidence for ionization stratification of the BLR: lines that are stronger in more highly ionized gases arise closer to the central source, which is not a surprising result. But is also clear why the photoionization equilibrium prediction of the size was so far off: the C IV and C III] lines arise in different parts of the BLR and their flux ratio is not a meaningful model constraint. The particle density in the C IV-emitting zone is apparently high enough that the C III] line is collisionally suppressed or the C III] emissivity is low for some other reason.

Time-delay measurements are available for multiple emission lines for only a bare handful of AGNs (see Peterson et al. 2004 for a compilation), but they all show a consistent pattern of ionization stratification.

[7] In X-ray astronomy, this quantity is often referred to as "excess variance," i.e., the variance above what is expected based on measurement uncertainties alone.

Measurements of Balmer-line lags are available for about three dozen AGNs that represent a wide range in luminosity. A major advance occurred with the measurement of Balmer-line lags for a sample of PG quasars[8] (Kaspi et al. 2000); this sample not only doubled the number of AGNs for which reverberation measurements were available, but it also significantly extended to higher values the luminosity range of reverberation-mapped AGNs. This allowed the first clear detection of the relationship between the broad-line region radius and the luminosity of the central source, although of course this relationship had been long anticipated (e.g., Koratkar & Gaskell 1991 and references therein).

It is often stated that it was the extension of the luminosity range to quasars that allowed the detection of the radius-luminosity relationship, but this is rather misleading. It is closer to the truth to say that the *R-L* relationship became detectable with the addition of the PG quasars because of the relatively small contribution from the host-galaxy starlight in these more luminous objects. In the case of the low-luminosity AGNs, the relatively nearby Seyfert galaxies, the high-precision flux measurements needed for reverberation mapping necessitated using fairly large spectrograph entrance apertures to mitigate against seeing effects (see Peterson et al. 1995). Therefore all of the optical-band flux measurements of Seyfert galaxy nuclei are strongly contaminated by starlight from the host galaxy. With no standard aperture geometry established, the amount of contamination varies significantly among the low-luminosity AGNs, thus introducing a great deal of scatter into the *R–L* relationship.

Bentz et al. (2006a) have attempted to assess the stellar contamination of the AGN continuum flux measurements by using high resolution images of reverberation-mapped AGN from the High Resolution Channel of the Advanced Camera for Surveys on *HST*. The combination of high angular resolution, a stable point-spread function, and unsaturated images allows removal of the central point source, the AGN itself, from the image, thus isolating the host galaxy. The amount of starlight that affects the AGN luminosity measurements can then be determined by synthetic aperture photometry, by measuring the galaxy flux collected through the spectrograph aperture used in the original monitoring campaign. The results are illustrated in Figure 3. Removal of the contaminating starlight flux from the AGN continuum flux measurements displaces the lower-luminosity points to the right in this diagram, flattening the slope of the relationship from the Kaspi et al. (2000) value

[8] "PG" or "Palomar–Green" quasars are those from the Bright Quasar Survey (Schmidt & Green 1983).

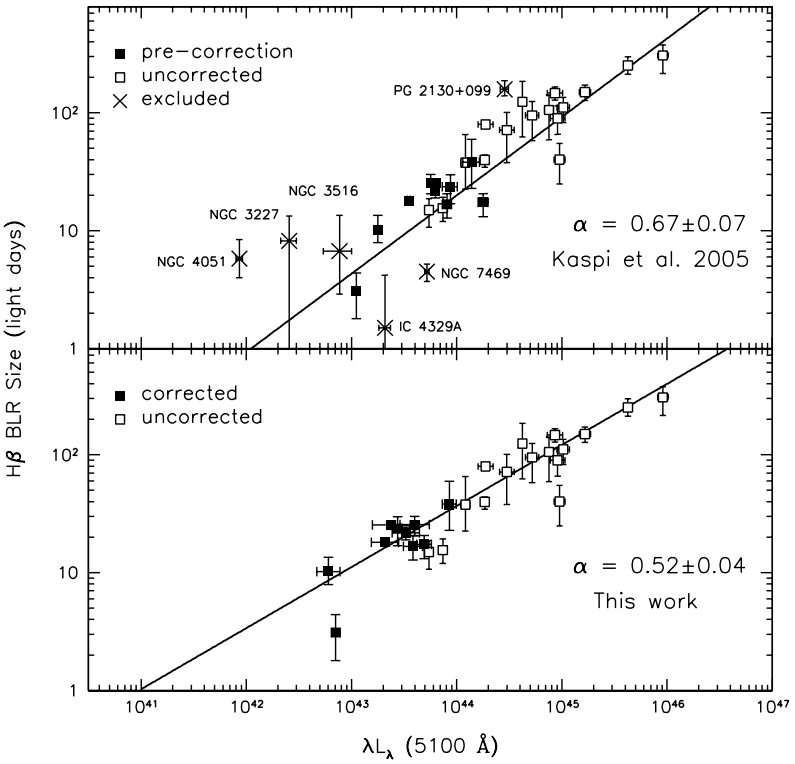

Fig. 3. Relationship between the BLR radius, as determined from the reverberation lag of Hβ, and the optical continuum luminosity. The top panel shows the relationship without correction for the host-galaxy contribution to the luminosity. In the bottom panel, a correction for the host-galaxy starlight contribution has been made for many of the lower-luminosity objects. The open squares are from Kaspi et al. (2005) and the filled squares are for the same AGNs, but after correction for starlight. Objects indicated by an $\times$ are not included in the fits, since host-galaxy models were not yet available. From Bentz et al. (2006a).

of $\alpha \approx 0.7$ to a value closer to $\alpha \approx 0.5$.

The R–L slope has been determined only for the Balmer emission lines. Until relatively recently, the few C IV lags that had been measured were bunched too closely in luminosity to determine the slope. However, recent measurements of the C IV response in the dwarf Seyfert galaxy NGC 4395 (Peterson et al. 2005), where the lag is about 1 hour, and the high-luminosity quasar S5 0836+71 (Kaspi et al. 2007), where the rest-frame lag is about 188 days, extend the luminosity range enough to see that $\alpha \approx 0.5$ appears to hold for C IV as well.

As noted earlier, continuum variations have more power at higher temporal frequencies: in other words, continuum variations are larger on time scales much longer than the light-travel time across the BLR. It is thus possible for an AGN to have quite different mean fluxes during different reverberation-mapping campaigns. This is indeed the case, with the best example being NGC 5548, which was spectroscopically monitored closely for 14 years (see

Peterson et al. 2002 and references therein). A different Hβ lag was measured for each year[9]. The Hβ lags for NGC 5548 vary between 6 and 26 days and the lag is well-correlated with the mean continuum luminosity. In this case, the "intrinsic" R–L relationship for NGC 5548 is $R \propto L_\lambda(5100\,\text{Å})^\beta$, where $\beta = 0.66 \pm 0.13$ (Bentz et al. 2007). The relatively steep slope of this relationship, however, is explained by the fact that the optical continuum varies with a lower amplitude than does the ionizing continuum. Comparing contemporaneous measurements of the optical and UV continuum shows that $L_\lambda(5100\,\text{Å}) \propto L_\lambda(1350\,\text{Å})^{0.84}$, so $R \propto L_\lambda(1350\,\text{Å})^{0.55}$. An alternative analysis by Cackett & Horne (2006) treats the BLR radius as a dynamic quantity that varies with luminosity and time. They find shallower relationship, $R \propto L_{\rm UV}^{0.13}$, partly because of a different assumption about the contribution of the host-galaxy light, but which is nevertheless closer to theoretical predictions of Korista & Goad (2004), i.e., $R \propto L_{\rm UV}^{0.23}$.

This can appear to be rather puzzling: how does the size of the BLR change so rapidly from year to year? How does the BLR know where it is supposed to be? The answer seems to be fairly obvious: there is emission-line gas everywhere in the BLR, probably from the outer accretion disk out to the dust-sublimation radius. However, the reverberation signal is dominated by the gas for which the *responsivity* is highest, i.e., under physical conditions (U and n_H) that give the largest marginal increase in the emissivity of a particular line as the continuum flux changes from L to $L+\delta L$. Conceptually, this is consistent with the "locally optimally emitting cloud (LOC)" model for the BLR (Baldwin et al. 1995), although it must be stressed that a fully consistent photoionization equilibrium model has still not been achieved.

Both recombination lines (like the Balmer lines) and collisionally excited lines (like C IV λ1549) have well-defined reverberation responses. The optical Fe II blends, strong features just shortward and longward of the Hβ+[O III] complex, do not: the optical Fe II lines clearly vary with the continuum, but cross-correlation of their light curves with the continuum light curves fail to yield a well-defined lag (Vestergaard & Peterson 2005; Kuehn et al. 2008). This may be an indication that the peak marginal response of the myriad of Fe II lines is not as sensitive to U and n_H as the other lines; in other words, the Fe II

[9] A common question is why Hβ has been the emission line of choice in ground-based reverberation mapping experiments, since Hα has the advantages of being stronger and less blended with other broad lines. The answer is twofold: first, the dilution of the continuum by starlight is less at shorter wavelengths, making the detection of low-level variability easier, and second, the proximity of the strong [O III] $\lambda\lambda$4959, 5007 doublet is crucial for accurate relative spectrophotometry. These lines do not vary on short timescales because of the large light-travel time across the narrow-line region (hundreds of years or more) and long recombination time (thousands of years) for such low-density gas. They therefore serve as an internal flux calibrator that allows relative spectrophotometry at 1–2% accuracy.

response is not very localized in the BLR.

4 Masses of Supermassive Black Holes

4.1 Masses from Reverberation Mapping

Masses of astronomical objects are measured by how they accelerate nearby matter. To determine the masses of black holes in the nuclei of galaxies, we can model the dynamics of either stars or gas in the vicinity of the black hole. The advantage of using stellar dynamics is that stars respond only to gravitational forces. The corresponding disadvantage is that high angular resolution is required since we must resolve the black hole radius of influence, as noted earlier, so this can be done only in relatively nearby systems. On the other hand, there is an advantage to using gas dynamics because gas can be found in close proximity to the nucleus and, as we discuss below, does not necessarily require high angular resolution. The corresponding disadvantage, of course, is that gas can also be accelerated by non-gravitational forces, such as radiation pressure or magnetic fields.

Woltjer (1959) was the first to suggest that AGN emission lines have large widths because the line-emitting gas is moving in a deep gravitational potential. If indeed the primary force acting on the gas is gravity, then the mass of the central object can be obtained from the virial equation by combining the line width ΔV with the size of the line-emitting region R as

$$M_{\rm BH} = \frac{f \Delta V^2 R}{G}, \tag{18}$$

where G is the gravitational constant and f is a dimensionless factor of order unity that depends on the geometry and dynamics of the gas, and unless the line-emitting region is spherically symmetric, the inclination of the system relative to the observer. What Woltjer did not have was the size of the line-emitting region: he knew only that the line-emitting region was unresolved, so $R < 100\,{\rm pc}$, and that the presence of forbidden lines required a maximum particle density and therefore a minimum volume [10], requiring $R > 1\,{\rm pc}$. This suggested that masses of order 10^8–$10^{10}\,M_\odot$ were present in AGNs.

By the 1970s, there were estimates of the size of the BLR from photoionization equilibrium calculations, as described earlier. But because the predicted BLR

[10] Recall that the distinction between the BLR and NLR was made much later by Khachikian & Weedman (1974).

sizes were an order of magnitude too large, the masses inferred were also an order of magnitude too large. My own suspicion is that this had a lot to do with the development of radiation-pressure driven outflow models of the BLR that were popular at the time (e.g., Blumenthal & Mathews 1975), since gravitationally bound gas would require central masses that were uncomfortably large.

It was not until the advent of reverberation mapping, however, that it was possible to obtain reliable sizes for the BLR and thus reliable masses. Indeed, recognition of this was slow, as a necessary (though not sufficient) condition for reverberation masses to be considered reliable is that each of the emission lines must yield the same mass, or, more specifically $R \propto \Delta V^{-2}$. The initial investigation (Krolik et al. 1991) of this "virial relationship" was not encouraging [11] . More recent analyses, however, find that the data are consistent with a virial relationship in every AGN for which it can be critically tested (Peterson & Wandel 1999, 2000; Onken & Peterson 2003; Kollatschny 2003a). The results for NGC 5548, the best studied AGN in this regard, are shown in Figure 4.

Given our lack of understanding of the actual geometry and kinematics of the BLR, we stick to simple parameterizations, and characterize what is undoubtedly a complex region by two very simple quantities, namely reverberation lag and line width. There are two different line width measures in use, FWHM and line dispersion $\sigma_{\rm line}$ (equation 16), with the former used more commonly. They both have advantages and disadvantages: FWHM is less sensitive to the line wings that might be lost by blending with other lines, but more sensitive to the presence of a central narrow component (or our ability to accurately account for it). The line dispersion, however, is well-defined for any profile [12] and much more useful for low-contrast lines, but is very sensitive to continuum placement. Peterson et al. (2004) argue that the best consistency with the virial relationship is found by (a) using $\sigma_{\rm line}$ as the line width measure and (b) measuring the line width in only the *variable* part of the emission line. They isolate the variable part of the emission line by combining the spectra used to measure the time delays into a mean spectrum and an rms spectrum: the non-variable components, such as the host galaxy spectrum and the narrow emission lines, do not appear in the rms spectrum, leaving only the variable parts of the emission lines. Collin et al. (2006) also argue that use of FWHM

[11] The principal problem with the Krolik et al. analysis was use of the DCF, as described earlier, which introduced discretization noise: all of the measured lags were multiples of 4 days, the sampling interval in the *IUE* observations of NGC 5548, and most of the lags are actually rather small (Table 1). Other problems include use of lines for which the lags were unreliable, either because the lines are weak and the measurements noisy, or because of aliasing resulting from the quasi-periodic continuum variations in NGC 5548 during that particular year.

[12] For example, how does one measure FWHM for a double-peaked profile?

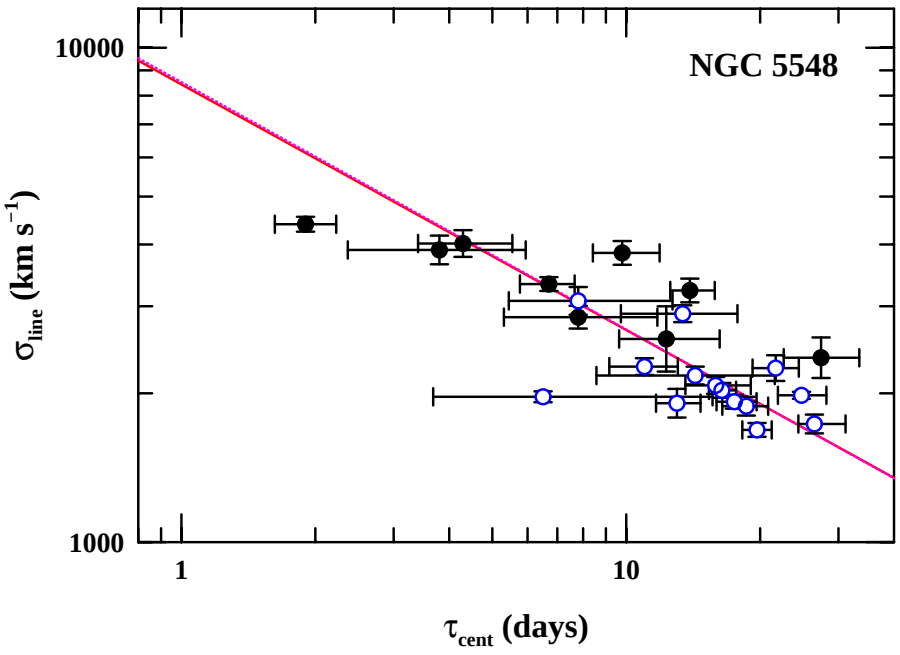

Fig. 4. Relationship between line width and lag for emission lines in NGC 5548. Open circles represent various measurements of the Hβ line over a 14 year period, closed circles represent other broad lines. The best-fit line to these data is also shown and has a slope consistent with the virial prediction $\sigma_{\rm line} \propto \tau^{-1/2}$. From Peterson et al. (2004).

introduces systematic difficulties that $\sigma_{\rm line}$ seems to avoid.

4.2 The Relationship Between Black Hole Mass and Bulge Velocity Dispersion

Another indication that reverberation-based black hole masses are reliable is that AGNs, like quiescent galaxies, show a clear $M_{\rm BH}$–σ_* relationship (Gebhardt et al. 2000b; Ferrarese et al. 2001; Onken et al. 2004; Nelson et al. 2004). Onken et al. (2004) use the $M_{\rm BH}$–σ_* relationship to calibrate the reverberation-mapping mass scale. They do this by assuming that the $M_{\rm BH}$–σ_* relationship is identical for AGNs and quiescent galaxies and then determining the mean value of the scale factor in equation (18) that yields the same normalization, as shown in Figure 5. The value they adopt is $\langle f \rangle = 5.5 \pm 1.8$, using $\sigma_{\rm line}$ as the line-width measure. Note that adopting a mean value for f is a *statistical correction*, since the scaling factor varies from one AGN to the next: use of a single value should thus lead to equal numbers of overestimated and underestimated masses. It may also seem surprising that the mean value f is so

large as a value closer to unity should be expected. This may be a projection effect: according to unified models, we see type 1 AGNs preferentially at low inclination, between $i = 0^{\rm o}$ (face-on) and some maximum angle $i_{\rm max}$ that is based on the relative space density of type 1 and type 2 AGNs. If the BLR motions are larger in the disk plane than in the polar direction, the projection factor will be larger for AGNs seen at low inclination, i.e., f will be larger for a given black hole mass. Unfortunately, it is rare that we have any way to determine the inclination at which we observe any particular AGN. However, we can distinguish lower-inclination radio sources from higher-inclination radio sources from their morphology: lower-inclination sources are core-dominated and higher-inclination sources are lobe-dominated. Wills & Browne (1986) argue that core-dominated sources statistically have narrower emission lines than lobe-dominated sources, which would indicate that the projection factors are, as expected, larger for low-inclination sources[13]. Jarvis & McLure (2006) further support this interpretation by comparing the radio spectral index (which is steep for lobe-dominated sources and flat for core-dominated sources) with line width, and reach the same conclusion.

Given how tight the $M_{\rm BH}$–σ_* relationship is in quiescent galaxies (Ferrarese & Merritt 2000; Gebhardt et al. 2000a), the scatter around the AGN $M_{\rm BH}$–σ_* relationship is probably the best measure of the typical systematic uncertainties in the reverberation-based mass measurements. This suggests that the typical errors are at the level of a factor of ~ 3. This is consistent with the differences in line widths between the different radio morphologies and spectral indices mentioned above.

4.3 Comparison of Reverberation-Based Masses with Masses from Gas and Stellar Dynamics

Of course, the most critical test of the validity of reverberation-based masses is direct comparison with other methods. Unfortunately, this is very difficult because the other major methods, modeling of gas dynamics and stellar dynamics, require high spatial resolution and must contend with the glare of the AGN itself on the same small scales. Only two reverberation-mapped AGNs, NGC 3227 and NGC 4151, are near enough and have black holes large enough that the black hole radius of influence is barely resolvable with current technology, $0\farcs12$ for NGC 3227 and $0\farcs31$ for NGC 4151. Mass measurements from gas dynamics and stellar dynamics are available for both of these galaxies, as summarized in Table 2. While these are not high precision measurements, there is

[13] The narrowest "broad lines" are those in NLS1s, of course, and these typically have widths larger than 1000 km s^{-1}. Because there are no AGNs with even narrower lines, there is no escaping the conclusion that the BLR has a significant velocity component in the polar direction.

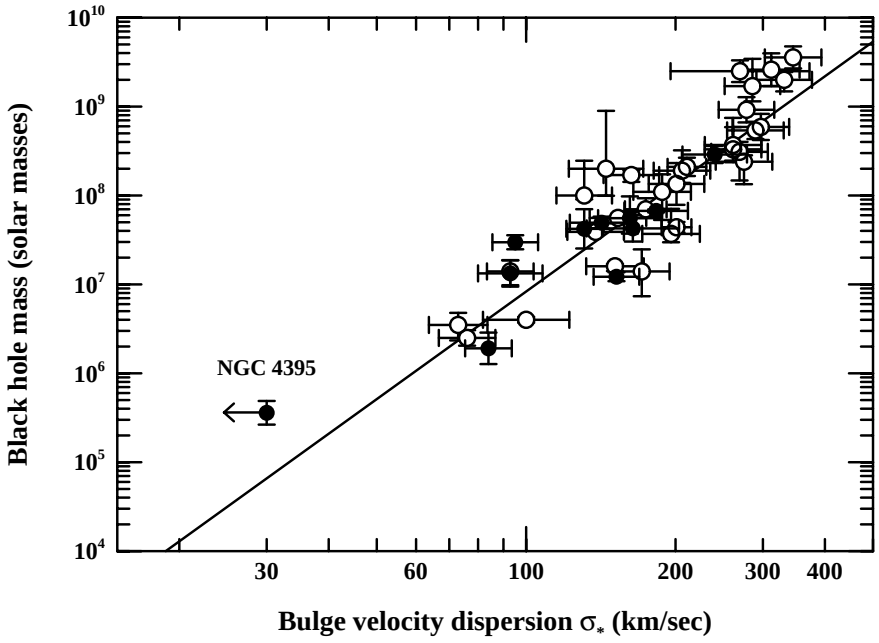

Fig. 5. Relationship between the black hole mass and host-galaxy stellar bulge velocity dispersion for reverberation-mapped AGNs. The two lines are best-fits to the quiescent galaxy data from Tremaine et al. (2002) (shallower line) and Ferrarese (2002) (steeper line). This is an updated version of a similar plot from Onken et al. (2004) which incorporates additional data from Nelson et al. (2004), Bentz et al. (2006b, 2007), and Denney et al. (2006). For these data (excluding NGC 4395) the adopted scaling factor is $f = 5.9 \pm 1.8$.

general agreement among the various methods. It should also be noted that since we use the mean scale factor $\langle f \rangle = 5.5$ for the reverberation masses, we cannot expect agreement to better than a factor of a few for individual AGNs.

4.4 The Relationship Between Black Hole Mass and Bulge Luminosity

A final consistency check is provided by the relationship between the central black hole mass and the host-galaxy bulge luminosity or bulge mass. We are using the same *HST* ACS images we obtained to determine the host-galaxy contribution to the AGN luminosity mentioned above (Bentz et al. 2006a) to investigate this. While this is a work in progress, we find general agreement between active and quiescent galaxies.

Table 2
Supermassive Black Hole Mass Measurements

Galaxy	Method	$M_{\rm BH}/10^6\,M_\odot$	Reference
NGC 3227	Reverberation	42 ± 21	1
	Gas dynamics	20^{+10}_{-4}	2
	Stellar dynamics	7–20	3
NGC 4151	Reverberation	46 ± 5	4
	Gas dynamics	$30^{+7.5}_{-2.2}$	2
	Stellar dynamics	≤ 70	5

References:

1: Peterson et al. (2004)

2: Hicks & Malkan (2007)

3: Davies et al. (2006)

4: Bentz et al. (2006b)

5: Onken et al. (2007)

4.5 The Relationship Between Black Hole Mass and AGN Luminosity

In Figure 6, we show the relationship between black hole mass and AGN luminosity for the reverberation-mapped AGNs. Important points to note are:

(1) All of these AGNs are accreting at sub-Eddington rates ($\dot{m} < 1$), typically at $\dot{m} \approx 0.1$.
(2) The NLS1s fall along the high $\dot{m}$ side of the distribution.
(3) At least some of the outliers at low $\dot{m}$ (e.g., NGC 3227) show evidence for significant internal reddening for which no correction has been attempted. Their luminosities (and hence accretion rates) are probably underestimated.

These reverberation-mapped AGNs anchor the AGN black hole mass scale.

4.6 Black Hole Masses from Scaling Relationships

Strong correlations between black hole masses and properties of the host galaxies — the bulge luminosity, mass, and velocity dispersion, in particular — not

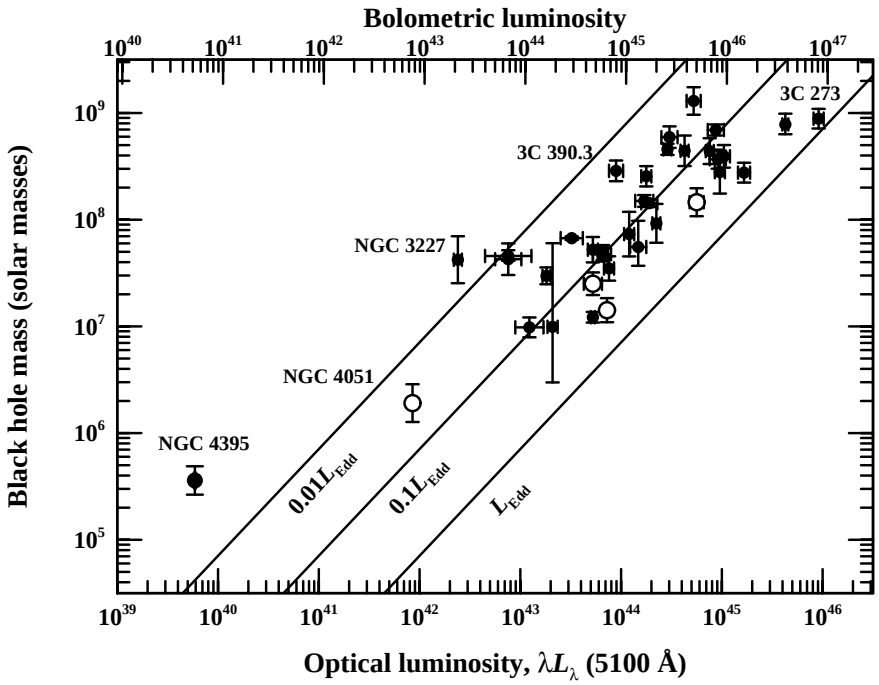

Fig. 6. The black hole mass–luminosity relationship for the reverberation-mapped AGNs. The open circles identify NLS1s, which are thought to be high Eddington ratio objects. The bolometric scale on top assumes that $L_{\rm bolometric} = 9\lambda L_\lambda(5100\,\text{Å})$. This is an updated version of Fig. 8 of Peterson et al. (2005), with revised masses for NGC 4151 (Bentz et al. 2006b) and NGC 4593 (Denney et al. 2006).

only provide us with useful constraints on galaxy formation and black hole growth, but are of practical use in determining black hole masses in systems where the direct methods cannot be brought to bear. Of course, in AGNs, measurement of any of the host-galaxy bulge properties is difficult. Fortunately, however, we can make use of the excellent correlation between the AGN continuum luminosity and BLR size to obtain the BLR radius without the resource-intensive method of reverberation mapping. By combining this size estimate with the width of the appropriate emission line, it is possible to estimate the mass of the black hole by using a single AGN spectrum. Of course, great care must be exercised in using scaling relationships to estimate the black hole mass: blending of lines (including narrow-line components) is a potentially serious problem, for example. Various versions of mass estimation based on various strong emission lines have been published (e.g., Wandel, Peterson, & Malkan 1999; McLure & Jarvis 2002; Vestergaard 2002, 2004; Shields et al. 2003; Green & Ho 2005; Vestergaard & Peterson 2006; Woo et al. 2006; Kollmeier et al. 2006; Collin et al. 2006; Netzer & Trakhtenbrot 2007; Treu et al. 2007; Salviander et al. 2007). A recent compilation by McGill et al. (2008) provides a detailed comparison of many of these. At the present time, it is probably safe to say that, if properly applied, scaling relationships yield

black hole masses that are accurate to a factor of 4–5.

4.7 New Challenges

Without a doubt, the single biggest source of uncertainty in determining black hole masses by either reverberation mapping or scaling relationships is the unknown inclination of the system. There are relatively few indicators of inclination:

(1) As noted earlier, in radio-loud AGNs, lower inclination sources can be distinguished from higher-inclination sources by radio spectral index or by radio morphology.
(2) Spectropolarimetry of the broad lines can reveal near-field scattering, which requires at least moderate inclination (Smith et al. 2002).
(3) In the case of the relatively few AGNs that have the double-peaked Balmer lines that are characteristic of a rotating disk (e.g., 3C 390.3), a model-dependent fit to the profile can yield an inclination.
(4) In the case of the relatively few AGNs that have superluminal jets (e.g., 3C 120), an upper limit to the inclination can be inferred

It has been suggested by a number of authors (Wu & Han 2001; Zhang & Wu 2002; McLure & Dunlop 2001) that inclination might be deduced by comparing the reverberation mass (which is inclination dependent) with the black hole mass predicted by the $M_{\rm BH}$–σ_* relationship (which is expected to be independent of inclination). While this might prove to be true statistically, individual cases where there is some indicator of inclination do not support this. In the case of 3C 120, where a superluminal jet indicates that $i < 20^{\rm o}$, the reverberation mass and the mass predicted by the $M_{\rm BH}$–σ_* relationship are virtually identical. If the BLR is a flat disk (which it surely is not), projection effects should lead to an order-of-magnitude difference between the two. In the case of Mrk 110, an independent mass estimate that should not be inclination dependent is available from gravitational redshifting of the emission lines is $M_{\rm grav} \approx 1.4\ (\pm 0.3) \times 10^7\, M_\odot$ (Kollatschny 2003b), while the reverberation mass is $M_{\rm rev} \approx 2.5\ (\pm 0.6) \times 10^7\, M_\odot$. Both of these are considerably larger than the $M_{\rm BH}$–σ_* prediction of $4.8 \times 10^6\, M_\odot$. Unfortunately, this does not look like a very promising way to determine inclination, at least not at this time, based on very sparse data.

The still unmet challenge facing reverberation mapping is to obtain a velocity-delay map for the BLR: even a map for *one* emission line in *one* AGN would be an important proof-of-concept. Of course, just a quick look back at Table 1 tells us that it will take at least a few different emission lines to hope to obtain a velocity-delay map of the entire BLR. Extensive simulations by Horne et al.

(2004) demonstrate that a velocity-delay map is well within current technical capabilities. High-fidelity velocity-delay maps will reveal the geometry, kinematics, and inclination of the system, leading to an understanding of how AGNs are fueled, how gas is simultaneously ejected from the system, and, to high accuracy, the mass of the central black hole.

5 The Future at High Resolution

While the theme of this school has been AGNs at high angular resolution, I have said very little about how our understanding of the central regions of AGNs stands to improve with the advent of new technologies such as interferometry in the near IR. This is largely because spatially resolving the BLR and accretion disk will remain a considerable challenge into the future. Since both the BLR radius and apparent brightness of nearby AGNs scale approximately like $L^{1/2}$, the apparently brightest AGNs will have BLRs with the largest angular size. NGC 4151 is one of the very brightest AGNs and the BLR, as traced by the Hβ line, has a radius of 6.6 light days (Bentz et al. 2006b), which projects to only 80 μarcseconds. Of course, if it becomes possible to resolve the BLR spatially at fairly high spectral resolution, combining this information with a velocity-delay map would significantly reduce any ambiguity about the structure and kinematics of the BLR (cf. Karovska & Elvis 2002). However, I think it is much more likely that answers will found well before this particular methodology is mature, probably from a less expected direction, such as gravitational microlensing (e.g., Poindexter, Morgan, & Kochanek 2008).

On the other hand, modest improvements in angular resolution could potentially have a huge impact in separating the AGN proper from the host galaxy, allowing study of the hosts in greater detail. An order of magnitude improvement in angular resolution would allow us to resolve the black hole radius of influence in most of the reverberation-mapped AGNs and thus use stellar dynamics to model the black hole masses and effect a direct comparison with reverberation-based masses.

Acknowledgments

The author is grateful to the organizers for the invitation to the school and to the students and other lecturers for stimulating conversations. Some of the work described here is supported at The Ohio State University by the US National Science Foundation through grant AST–0604066 and by NASA through grants GO-10516 and AR-10691 from the Space Telescope Science Institute.

References

Alexander, T. 1997, in Astronomical Time Series, ed. D. Maoz, A. Sternberg, & E.M. Leibowitz (Dordrecht: Kluwer), p. 163

Ambartsumian, V.A. 1971 in Nuclei of Galaxies, ed. D.J.K. O'Connell (New York: American Elsevier), p. 1

Andrillat, Y., & Souffrin, S. 1968, ApLetters, 1, 111

Antokhin, I.I., & Bochkarev, N.G. 1983, Soviet Astron., 27, 261

Antonucci, R.R.J., & Cohen, R.D. 1983, ApJ, 271, 564

Bahcall, J.N., Kozlovsky, B.-Z., & Salpeter, E.E. 1972, ApJ, 171, 467

Baldwin, J.A., Ferland, G.J., Korista, K.T., & Verner, D. 1995, ApJ, 455, L119

Bentz, M.C., Peterson, B.M., Pogge, R.W., Vestergaard, M., & Onken, C.A. 2006a, ApJ, 644, 133

Bentz, M.C., et al. 2006b, ApJ, 651, 775

Bentz, M.C., et al. 2007, ApJ, 662, 205

Blandford, R.D. 1992, in Relationships Between Active Galactic Nuclei and Starburst Galaxies, ASP Conf. Series Vol. 31,(San Francisco: ASP), p. 455

Blandford, R.D., & McKee, C.F. 1982, ApJ, 255, 419

Blumenthal, G.R., & Mathews, W.G. 1975, ApJ, 198, 517

Cackett, E., & Horne, K. 2006, MNRAS, 365, 1180

Capriotti, E.R., Foltz, C.B., & Peterson, B.M. 1982, ApJ, 261, 35

Clavel, J., et al. 1991, ApJ, 366, 64

Collin-Souffrin, S. 1991, A&A, 249, 344

Collin, S., Kawaguchi, T., Peterson, B.M., & Vestergaard, M. 2006, A&A, 456, 75

Courvoisier, T.J.-L., & Clavel, J. 1991, A&A, 248, 389

Davies, R.I., et al. 2006, ApJ, 646, 754

Denney, K.D., et al. 2006, ApJ, 653, 152

Edelson, R.A., & Krolik, J.H. 1988, ApJ, 33, 646

Elvis, M., & Karovska, M. 2002, ApJ, 581, L67

Fabrika, S.N. 1980, Soviet Astron. Lett., 6, 293

Ferland, G.J., & Mushotzky, R.F. 1982, ApJ, 262, 564

Ferrarese, L., & Merritt, D. 2000, ApJ, 539, L9

Ferrarese, L., et al. 2001, ApJ, 555, L79

Gaskell, C.M., & Peterson, B.M. 1987, ApJS, 65, 1

Gaskell, C.M., & Sparke, L.S. 1986, ApJ, 305, 175

Gebhardt, K., et al. 2000a, ApJ, 539, L13

Gebhardt, K., et al. 2000b, ApJ, 543, L5

Ghez, A.M., et al. 2005, ApJ, 620, 744

Green, J.E., & Ho, L.C. 2005, ApJ, 630, 122

Herrnstein, J.R., et al. 1999, Nature, 400, 539

Hicks, E.K.S., & Malkan, M. 2007, ApJS, 173, 31

Horne, K., Peterson, B.M., Collier, S., & Netzer, H. 2004, PASP, 116, 465

Kaspi, S., et al. 2000, ApJ, 533, 631

Kaspi, S., Maoz, D., Netzer, H., Peterson, B.M., Vestergaard, M., & Jannuzi, B.T. 2005, ApJ, 629, 61
Kaspi, S., Brandt, W.N., Maoz, D., Netzer, H., Schneider, D.P., & Shemmer, O. 2007, ApJ, 659, 997
Kawaguchi, T., Mineshige, S., Machida, M., Matsumoto, R., & Shibata, K. 2000, PASJ, 52, 1
Khachikian, E.Ye., & Weedman, D.W. 1974, ApJ, 192, 581
Kollatschny, W. 2003a, A&A, 407, 461
Kollatschny, W. 2003b, A&A, 412, 61
Kollmeier, J.A., et al. 2006, ApJ, 648, 128
Koratkar, A.P., & Gaskell, C.M. 1991 ApJ, 370, L61
Korista, K.T., & Goad, M.R. 2004, ApJ, 606, 749
Kormendy, J., & Richstone, D., 1995, ARAA, 33, 581
Krolik, J.H., Horne, K., Kallman, T.R., Malkan, M.A., Edelson, R.A., & Kriss, G.A. 1991, ApJ, 371, 541
Kuehn, C.A., Baldwin, J.A., Peterson, B.M., & Korista, K.T. 2008, ApJ, 673, 69
Lynden-Bell, D., 1969, Nature, 223, 690
Marconi, A., & Hunt, L.K. 2003, ApJ, 589, 21
McGill, K.L., Woo, J.-H., Treu, T., & Malkan, M.A. 2008, ApJ, 673, 703
McLure, R.J., & Dunlop, J.S. 2001, MNRAS, 327, 199
McLure, R.J., & Jarvis, M.J. 2002, MNRAS, 337, 109
Miyoshi, M., et al. 1995, Nature, 373, 127
Nelson, C.H., et al. 2004, ApJ, 615, 652
Netzer, H., & Trakhtenbrot, B. 2007 ApJ, 654, 754
Onken, C.A., & Peterson, B.M. 2002, ApJ, 572, 746
Onken, C.A., et al. 2004, ApJ, 615, 645
Onken, C.A., et al. 2007, ApJ, 670, 105
Osterbrock, D.E., & Pogge, R.W. 1985, ApJ, 297, 166
Peterson, B.M. 1993, PASP, 105, 247
Peterson, B.M. 1997, An Introduction to Active Galactic Nuclei, (Cambridge: Cambridge University Press), p. 1
Peterson, B.M. 2001, in Advanced Lectures on the Starburst–AGN Connection, ed. I. Aretxaga, D. Kunth, & R. Mújica (Singapore: World Scientific), p. 3
Peterson, B.M., & Wandel, A. 1999, ApJ, 521, L95
Peterson, B.M., & Wandel, A. 2000, ApJ, 540, L13
Peterson. B.M., et al. 1983, AJ, 88, 926
Peterson. B.M., et al. 1985, ApJ, 292, 164
Peterson, B.M., et al. 1991, ApJ, 368, 119
Peterson, B.M., et al. 1995, PASP, 107, 579
Peterson, B.M., et al. 1998, PASP, 110, 660
Peterson, B.M., et al. 2002, ApJ, 581, 197
Peterson, B.M., et al. 2004, ApJ, 613, 682
Peterson, B.M., et al. 2005, ApJ, 632, 799 (Erratum: 2006, ApJ, 641, 638)

Phillips, M.M. 1978, ApJS, 38, 187
Poindexter, S., Morgan, N., & Kochanek, C.S. 2008, ApJ, 673, 34
Reynolds, C.S., Young, A.J., Begelman, M.C., & Fabian, A.C. 1999, ApJ, 514, 164
Salpeter, E.E. 1964, ApJ, 140, 796
Sandage, A. 1965, ApJ, 141, 1560
Salviander, S., Shields, G.A., Gebhardt, K., & Bonning, E.W. 2007, ApJ, 662, 131
Schmidt, M. 1963, Nature, 197, 1040
Schmidt, M., & Green, R.F. 1983, ApJ, 269, 352
Schödel, R., Ott, T., Genzel, R., Eckart, A., Mouawad, N., & Alexander, T. 2003, ApJ, 596, 1015
Seyfert, C. 1943, ApJ, 97, 28
Shakura, N.I., & Sunyaev, R.A. 1973, A&A, 24, 337
Shields, G.A., Gebhardt, K., Salviander, S., Wills, B.J., Xie, B., Brotherton, M.S., Yuan, J., & Dietrich, M. 2003, ApJ, 583, 124
Smith, J.E., Young, S., Robinson, A., Corbett, E.A., Giannuzzo, M.E., Axon, D.J., & Hough, J.H. 2002, MNRAS, 335, 773
Tohline, J.E, & Osterbrock, D.E. 1976, ApJ, 210, L117
Treu, T.,Woo, J.-H., Malkan, M.A., & Blandford, R.D. 2007, ApJ, 667, 117
Ulrich, M.-H., et al. 1991, ApJ, 382, 483
Ulrich, M.-H., & Horne, K. 1996, MNRAS, 283, 748
Vestergaard, M. 2002, ApJ, 571, 733
Vestergaard, M. 2004, ApJ, 601, 676
Vestergaard, M., & Peterson, B.M. 2005, ApJ, 625, 688
Vestergaard, M., & Peterson, B.M. 2006, ApJ, 641, 689
Wandel, A., Peterson, B.M., & Malkan. M.A. 1999, ApJ, 526, 579
Weedman, D.W. 1976, QJRAS, 16, 227
White, R.J., & Peterson, B.M. 1994, PASP, 106, 879
Wills, B.J., & Browne, I.W.A. 1986, ApJ, 302, 56
Woltjer, L. 1959, ApJ, 130, 38
Woo, J.-H., Treu, T., Malkan, M.A., & Blandford, R.D. 2006, ApJ, 645, 900
Wu, X.-B., & Han, J.L. 2001, 561, 59
Zhang, T.-Z., & Wu, X.-B. 2002, ChJAA, 2, 487
Zel'dovich, Ya.B., & Novikov, I.D. 1964, Sov. Phys. Dokl., 158, 811